Cell, Vol. 99, 323–334, October 29, 1999, Copyright ©1999 by Cell Press

Crystal Structure of the PTEN Tumor Suppressor: Implications for Its Phosphoinositide Phosphatase Activity and Membrane Association

Jie-Oh Lee,[1,2,9] Haijuan Yang,[4,9] Maria-Magdalena Georgescu,[5,10] Antonio Di Cristofano,[3,10] Tomohiko Maehama,[6,10] Yigong Shi,[7] Jack E. Dixon,[6] Pier Pandolfi,[3] and Nikola P. Pavletich[1,2,8]

[1]Cellular Biochemistry and Biophysics Program
[2]Howard Hughes Medical Institute
[3]Department of Human Genetics and Molecular Biology Program
Memorial Sloan-Kettering Cancer Center
New York, New York 10021
[4]Department of Pharmacology
Sloan-Kettering Division
Joan and Sanford I. Weill Graduate School of Medical Sciences
Cornell University
New York, New York 10021
[5]Laboratory of Molecular Oncology
The Rockefeller University
New York, New York 10021
[6]Department of Biological Chemistry
University of Michigan
Ann Arbor, Michigan 48109
[7]Department of Molecular Biology
Princeton University
Princeton, New Jersey 08544

Summary

The *PTEN* tumor suppressor is mutated in diverse human cancers and in hereditary cancer predisposition syndromes. PTEN is a phosphatase that can act on both polypeptide and phosphoinositide substrates in vitro. The PTEN structure reveals a phosphatase domain that is similar to protein phosphatases but has an enlarged active site important for the accommodation of the phosphoinositide substrate. The structure also reveals that PTEN has a C2 domain. The PTEN C2 domain binds phospholipid membranes in vitro, and mutation of basic residues that could mediate this reduces PTEN's membrane affinity and its ability to suppress the growth of glioblastoma tumor cells. The phosphatase and C2 domains associate across an extensive interface, suggesting that the C2 domain may serve to productively position the catalytic domain on the membrane.

Introduction

Mutation of the tumor suppressor *PTEN/MMAC1* (Li et al., 1997; Steck et al., 1997) is a common event in diverse human cancers, occurring in about 50% of glioblastoma, endometrial carcinoma, prostate carcinoma, and melanoma cases (reviewed in Maehama and Dixon, 1999). In addition, germline mutations in *PTEN* are associated with the dominantly inherited Cowden and Bannayan-Zonana syndromes, which are characterized by the formation of multiple benign tumors and by the increased risk of malignant breast and thyroid tumors. Heterozygous disruption of *PTEN* in mice leads to neoplasia in multiple tissues reminiscent of human Cowden disease (Di Cristofano et al., 1998; Suzuki et al., 1998; Podsypanina et al., 1999; Sun et al., 1999).

Ectopic expression of PTEN in PTEN-null glioblastoma or renal cell carcinoma cells causes cell cycle arrest in the G1 phase (Furnari et al., 1998; Li and Sun, 1998). In immortalized PTEN-deficient mouse embryonic fibroblasts, PTEN can restore apoptosis induced by stimuli such as UV irradiation (Stambolic et al., 1998). And in NIH 3T3 fibroblasts, PTEN can suppress cell migration, spreading, and the formation of focal adhesions (Tamura et al., 1998).

The 403–amino acid PTEN protein contains the signature motif HCXXGXXR present in the active sites of protein tyrosine phosphatases (PTPs) and dual specificity protein phosphatases (DSPs), but it has little sequence homology to these protein families outside this motif. Rather, the amino-terminal 190–amino acid region of PTEN encompassing the signature motif has homology to tensin and auxilin (Li et al., 1997; Steck et al., 1997). Tensin is an actin-binding protein localized to focal adhesion complexes, and auxilin is involved in the uncoating of clathrin-coated vesicles. Beyond the tensin/auxilin/phosphatase homology domain, PTEN contains an ~220–amino acid carboxy-terminal region whose function has not been clear. Tumor-derived mutations map evenly to the two domains, and mutations in either domain have been shown to reduce or eliminate PTEN's growth suppression activity (Furnari et al., 1998; Georgescu et al., 1999).

PTEN can dephosphorylate tyrosine-, serine-, and threonine-phosphorylated peptides, and this activity requires highly acidic substrates (Myers et al., 1997). The focal adhesion kinase (FAK) has been shown to be a substrate of PTEN in vitro (Tamura et al., 1998). Recent studies have shown that PTEN can also dephosphorylate phosphatidylinositol (3,4,5)-trisphosphate ($PI(3,4,5)P_3$) in vitro, with specificity for the phosphate group at the D3 position of the inositol ring (Maehama and Dixon, 1998). $PI(3,4,5)P_3$ is a lipid second messenger produced by the phosphoinositide 3-kinase (PI3K) and activates downstream effectors. These include the Akt/PKB kinase that has potent antiapoptotic and growth stimulatory effects. A role for the $PI(3,4,5)P_3$ phosphatase activity of PTEN in its tumor suppressor function has been supported by several observations. Tumor cell lines with mutant PTEN have elevated levels of $PI(3,4,5)P_3$ and of Akt activity (Stambolic et al., 1998), and the introduction of wild-type PTEN reduces levels of both (Li and Sun, 1998). In *C. elegans*, a pathway that contains the PI3 kinase and Akt homologs also contains the DAF-18 gene that has homology to PTEN (Ogg and Ruvkun, 1998). Finally, the

[8]To whom correspondence should be addressed (e-mail: nikola@xray2.mskcc.org).
[9]These authors contributed equally to this work.
[10]These authors contributed equally to this work.

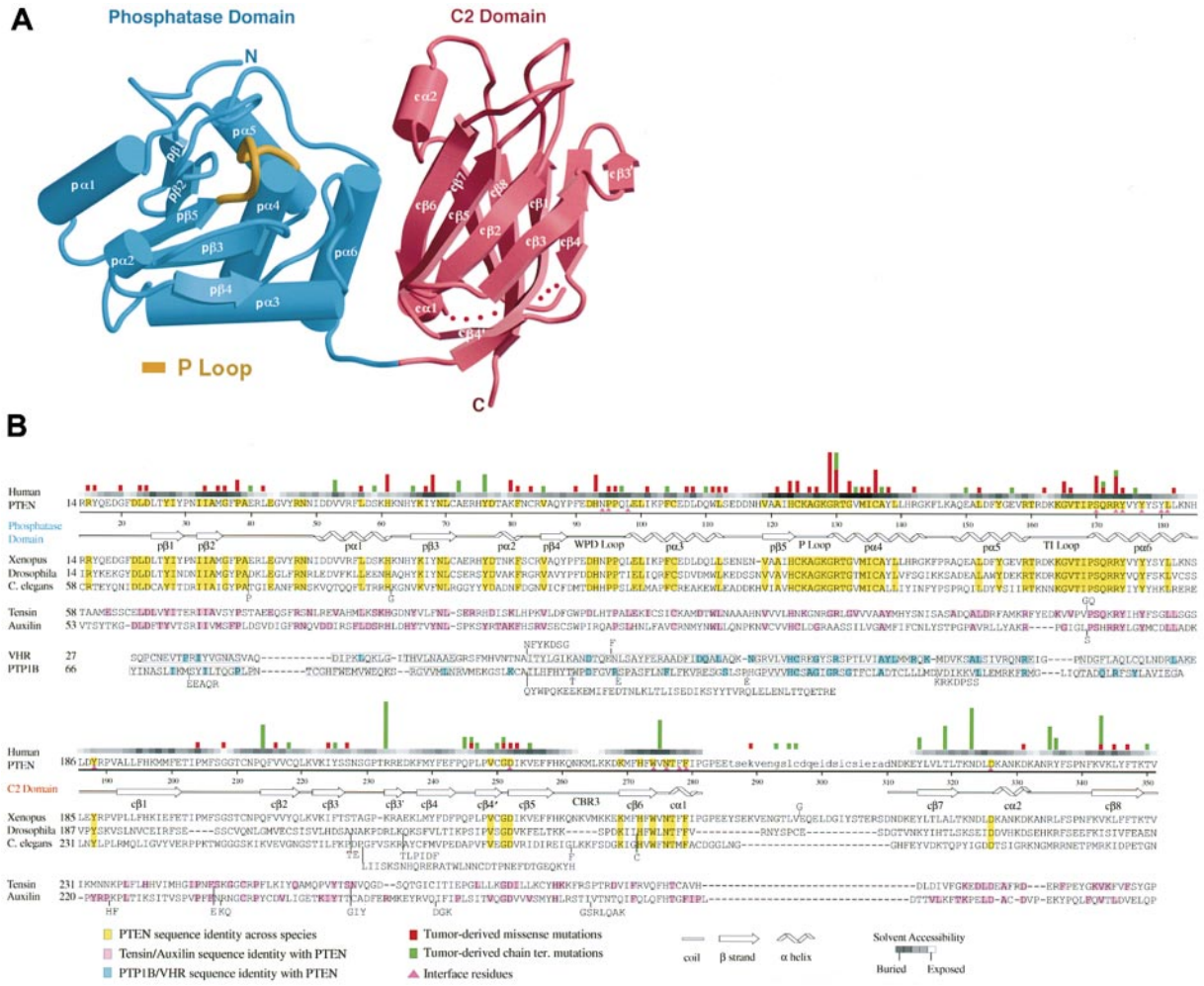

Figure 1. PTEN Has an N-Terminal Phosphatase Domain and a C-Terminal C2 Domain

(A) Overall view of the PTEN structure. The dotted line indicates the region deleted in the crystallized protein.

(B) Conservation of PTEN and histogram of 93 missense (red bars) and 80 chain termination (green bars) tumor-derived mutations. The alignment of C2 domains, obtained with the program PSI-BLAST (Altschul et al., 1997) and THREADER2 (Miller et al., 1996), may not be reliable outside regions of apparent sequence homology. The structural homology with the VHR and PTP1B phosphatase domains is indicated with boxes around VHR and PTP1B sequences, and the sequence identity is highlighted in blue. Residues in the deleted loop are shown in lowercase.

Gly129Glu tumor-derived mutation that maps to the phosphatase signature motif eliminates PTEN's lipid phosphatase activity but not its protein phosphatase activity (Furnari et al., 1998; Myers et al., 1998).

Here, we describe the 2.1 Å crystal structure of human PTEN bound to L(+)-tartrate (Figure 1A) and discuss the implications this structure, in conjunction with our in vitro membrane binding, mutagenesis, and growth suppression data, have for our understanding of PTEN's phosphatase activity, its association with the membrane, and its inactivation by mutations in cancer.

Results and Discussion

Structure Determination

Proteolytic digestion indicated that PTEN has unstructured or loosely folded regions of 7 and 49 residues at the N and C termini, respectively, and of 24 residues in an internal loop (residues 286–309; Figure 1B; data not shown). Initial crystals, obtained using PTEN truncated at its termini (residues 7–353), diffracted poorly. Therefore, the 24-residue protease-sensitive loop was also deleted from the recombinant clone. This truncated PTEN protein has in vitro PI(3,4,5)P_3 phosphatase activity similar to that of full-length PTEN (K_{cat}/K_M of 24.0 $min^{-1}mM^{-1}$ and 17.3 $min^{-1}mM^{-1}$ for truncated and full-length PTEN, respectively); its in vitro membrane affinity is comparable to that of full-length PTEN (discussed later); and its apoptosis inducing activity is essentially identical to that of full-length PTEN when transfected into LNCaP cells, a PTEN-deficient prostate cancer cell line (data not shown). The truncated PTEN was crystallized from Na/K L(+)-tartrate, and its structure was determined at 2.1 Å resolution. An L(+)-tartrate molecule, which inhibits the PTEN activity with a K_i of ~15 mM (data not shown), is bound in the active site (Figure 2D).

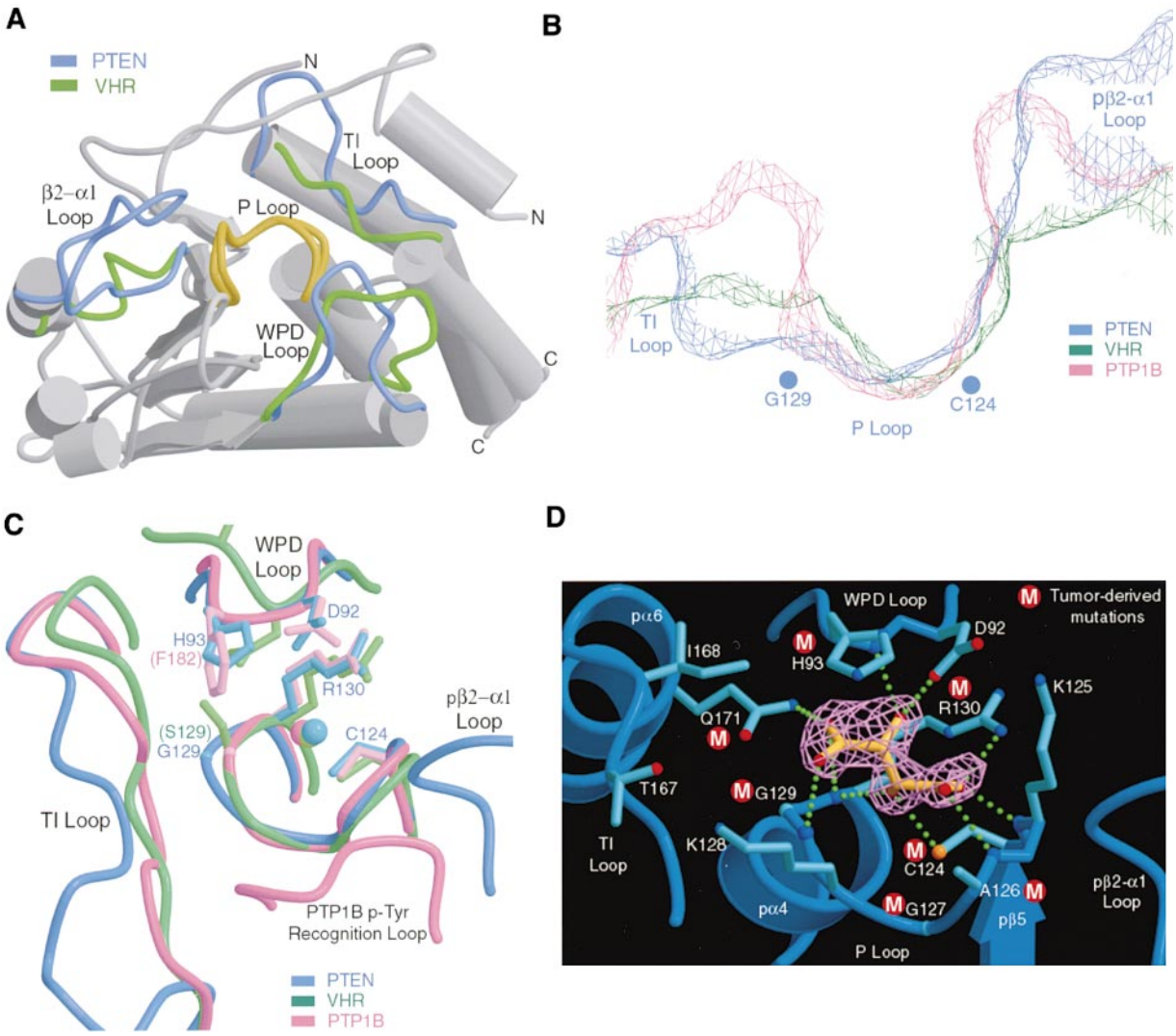

Figure 2. The PTEN Phosphatase Domain Has the Same Fold as the Dual Specificity Phosphatase VHR, but the Structure Differs around the Active Site

(A) Superimposition of the PTEN phosphatase domain and VHR structures. The structural elements around the active site that differ in the two structures—the pβ2-α1, "TI", and "WPD" loops—are in blue for PTEN and green for VHR.

(B) Slice of the active site molecular surface, represented as a wire mesh, shows the larger size of the PTEN active site pocket compared to VHR and PTP1B. View is rotated approximately 180° about the vertical axis of Figure 2A.

(C) Comparison of the active site structural elements and active site residues of PTEN, VHR, and PTP1B. Blue, green, and magenta spheres near the catalytic Cys-124 indicate the positions of a carboxylate carbon of tartrate in PTEN, the sulfur atom of sulfate in VHR, and the phosphorous atom of phosphotyrosine in PTP1B, respectively. PTEN residues are labeled, and residues of VHR and PTP1B are labeled only when they differ from PTEN. Orientation as in Figure 2B.

(D) Close-up view of the PTEN active site, showing the contacts made with the tartrate molecule (green dotted lines). Fo-Fc difference electron density around the tartrate molecule is shown in magenta. The map was calculated at 2.1 Å using a PTEN model before any tartrate atoms were built; it was contoured at 2.5 σ.

Overall Structure of PTEN

The PTEN structure consists of a 179-residue N-terminal domain (residues 7–185) and a 166-residue C-terminal domain (residues 186–351; Figures 1A and 1B). The N-terminal domain contains the PTP signature motif and has a structure similar to the dual specificity phosphatase VHR. However, the phosphatase active site of PTEN is larger than those of VHR and the protein tyrosine phosphatase PTP1B, and residues responsible for this structural feature are conserved in PTEN homologs. The larger size of the pocket would be important in accommodating a $PI(3,4,5)P_3$ substrate. The C-terminal domain has a structure similar to the C2 domain that mediates the Ca^{2+}-dependent membrane recruitment of several signaling proteins, such as the phosphoinositide-specific phospholipase Cδ1 (PLCδ1), phosphoinositide 3-kinase (PI3K), and protein kinase C (PKC) (reviewed in Rizo and Sudhof, 1998). The PTEN C2 domain lacks the canonical Ca^{2+} ligands, and in this respect it is similar to the C2 domains of the Ca^{2+}-independent PKC iso-

types (Rizo and Sudhof, 1998). The C2 and phosphatase domains associate across an extensive interface that is adjacent to the phosphatase active site and consists of conserved residues frequently mutated in cancer.

Structure of the Phosphatase Domain

The structure consists of a central five-stranded β sheet that packs with two α helices on one side and four on the other. This overall structure is similar to the dual specificity phosphatase VHR (Yuvaniyama et al., 1996), and the two structures can be superimposed with an rmsd of 1.75 Å for 121 Cα atoms (Figure 2A). There are several differences in the two structures, and some of these map near the active site. Relative to VHR, PTEN has an 11-residue insertion (residues 42–52) in the pβ2-α1 loop and a 4-residue insertion (residues 163–166) in the pα5-α6 loop (henceforth "TI" loop to reflect the conserved threonine and isoleucine residues) (Figures 1B and 2A). These PTEN insertions are also absent from the tyrosine phosphatase PTP1B structure (Jia et al., 1995), although the phospho-tyrosine recognition loop of PTP1B has a position similar to the PTEN pβ2-α1 insertion (Figure 2C).

Active Site Pocket

The PTEN HCXXGXXR signature motif forms a loop (P loop, residues 123–130) located at the bottom of the active site pocket, in common with PTPs and DSPs. The walls of the pocket are made up of side chain and backbone groups from the P loop, the pβ4-α3 loop (residues 91–94; "WPD" loop following the PTP1B nomenclature), and the "TI" loop. The PTEN pocket is ~8 Å deep with an elliptical opening of ~5 × 11 Å. Compared to VHR, the PTEN pocket is both wider and deeper; compared to PTP1B it is about twice as wide but has a similar depth (Figure 2B).

The larger width of the pocket compared to PTP1B and VHR is primarily due to the "TI" loop of PTEN. This loop, which contains a conserved 4-residue insertion relative to PTP1B and VHR, has a structure that is displaced away from the center of the pocket by several angstroms (Figure 2C). This results in an extension to the pocket, with the conserved Val-166–Thr-167–Ile-168 residues forming the side wall of this extension (Figure 2D). The "TI" loop has a rigid conformation stabilized by contacts to the rest of the phosphatase domain and is adjacent to the C2 domain. The larger width of the PTEN pocket is consistent with the larger size of the PI(3,4,5)P_3 substrate compared to phospho-tyrosine, serine, or threonine substrates. The importance of the pocket extension in PTEN's PI(3,4,5)P_3 phosphatase activity can be seen in the Gly129Glu tumor-derived mutation, which disrupts PTEN's PI(3,4,5)P_3 phosphatase activity but maintains the tyrosine phosphatase activity (Furnari et al., 1998; Myers et al., 1998). Gly-129 is at the bottom of the pocket, near the extension, and the structure suggests that this mutation would reduce the size of PTEN pocket extension (Figures 2B and 2C).

It has been suggested that the depth of the active site pocket is an important determinant of the phospho–amino acid specificity, the shallow pocket of VHR allowing both phospho-tyrosine and the shorter phospho-serine/threonine substrates to reach the catalytic cysteine at the bottom, while the deeper PTP1B pocket permitting only phospho-tyrosine to reach (Yuvaniyama et al., 1996). The wider opening of PTEN's pocket is consistent with its ability to dephosphorylate phospho-serine/threonine substrates in addition to phosphotyrosine (Myers et al., 1997).

Active Site Residues

In the PTEN HCXXGXXR motif, the Cys-124 and Arg-130 residues that are essential for catalysis and the His-123 and Gly-127 residues that are important for the conformation of the P loop (Barford et al., 1994; Stuckey et al., 1994) have the same position and conformation as in the PTP1B–substrate complex (Figures 2C and 2D). In addition, Asp-92 of the PTEN "WPD" loop is in an identical position as the corresponding PTP1B Asp-181 (Figure 2C), which serves as a general acid to facilitate protonation of the phenolic oxygen atom of the tyrosyl leaving group (Jia et al., 1995). Similar to the mammalian PTPs, mutation of Asp-92 to Ala in PTEN results in a 700-fold reduction in catalytic activity toward PI(3,4,5)P_3 (data not shown). These observations suggest that PTEN binds and hydrolyses the phosphate ester with a mechanism similar to that of PTP1B.

The P loop sequence of PTEN is unique among known PTPs in that it has two basic residues (Lys-125 and Lys-128) in its center. This PTEN motif, H-C-K/R^{125}-A-G-K^{128}-G-R, is conserved in yeast homologs of PTEN as well (reviewed by Maehama and Dixon, 1999). These lysine residues, together with His-93 of the "WPD" loop, also invariant across species, give the PTEN pocket a highly basic character that would be mostly absent from PTP1B or VHR (Figure 4C). The positive charge in the pocket is consistent with the negative charge of the PI(3,4,5)P_3 substrate and with PTEN's preference for highly acidic polypeptide substrates (Myers et al., 1997).

Bound Tartrate Molecule

At one end of the L(+)-tartrate molecule, a carboxylate group and the adjacent hydroxyl group bind over the active site Cys-124, making hydrogen bonds to backbone amide groups and to the side chains of the Cys-124 and Arg-130 of the P loop (Figure 2D). The carboxylate and hydroxyl groups are at a very similar position as the phosphate group of the phosphotyrosine substrate in PTP1B, and their contacts to the active site closely reproduce the array of contacts made by the phosphate group in the PTP1B–substrate structure (Jia et al., 1995).

The carboxylate and hydroxyl groups at the other end of the tartrate molecule bind in the part of the PTEN pocket that corresponds to an extension relative to the pockets of PTP1B and VHR, and partially fill this extension. This carboxylate group makes three hydrogen bonds with backbone amide groups on the P loop and the "WPD" loop, and with the Gln-171 side chain from the "TI" loop (Figure 2D). The adjacent hydroxyl group makes two more hydrogen bonds with a backbone amide group and Asp-92 side chain from "WPD" loop (Figure 2D). These interactions suggest that PTEN has a

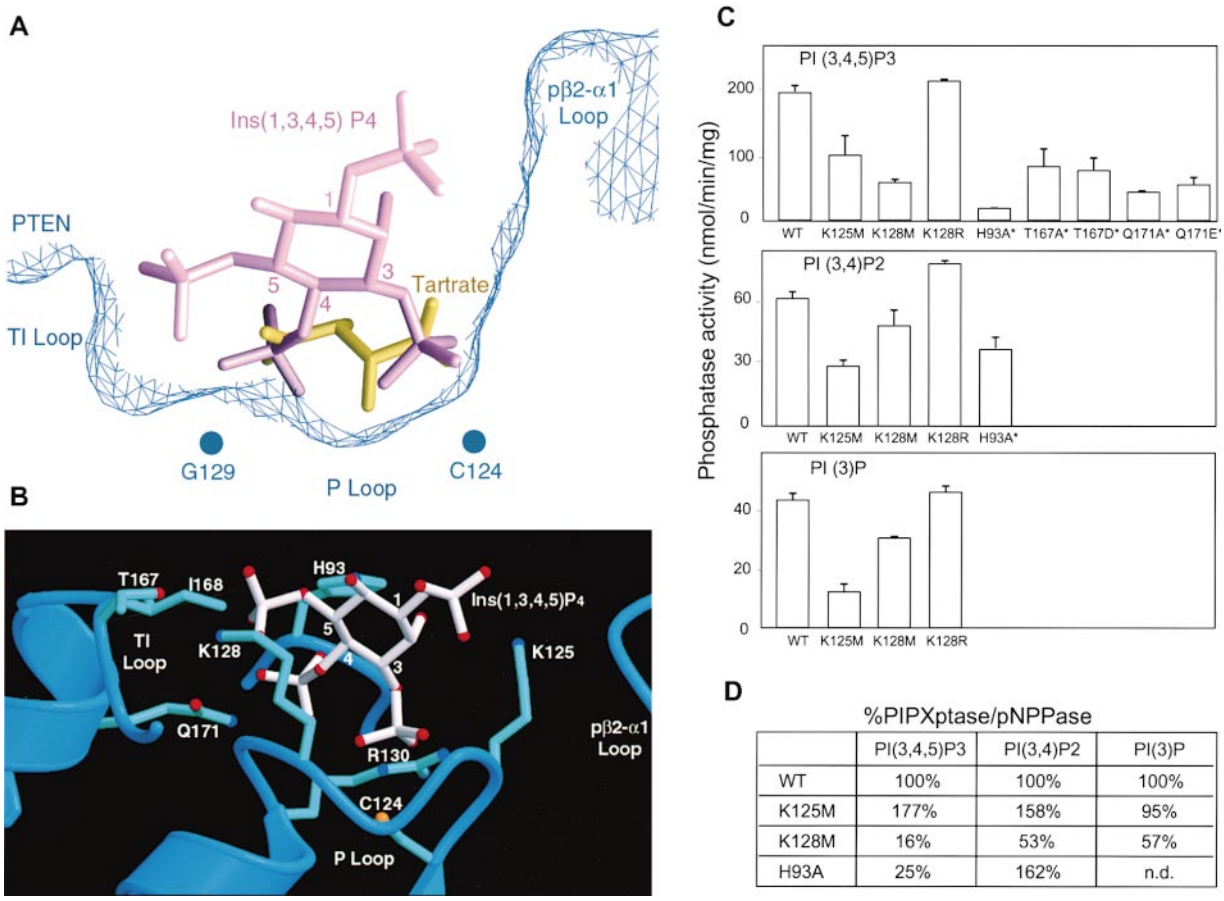

	PI(3,4,5)P3	PI(3,4)P2	PI(3)P
WT	100%	100%	100%
K125M	177%	158%	95%
K128M	16%	53%	57%
H93A	25%	162%	n.d.

Figure 3. Model of Ins(1,3,4,5)P_4 Binding to the PTEN Active Site

(A) The phosphate groups at the D3 and D4 positions of Ins(1,3,4,5)P_4 (PDB entry 1bwn) are superimposed on the carboxylate groups of the tartrate molecule bound in the PTEN active site. Orientation as in Figure 2B.

(B) Model of PTEN-Ins(1,3,4,5)P_4 complex. Side chains that are important for Ins(1,3,4,5)P_4 binding are shown.

(C) Lipid phosphatase activity of human PTEN mutants. PI(3,4,5)P_3 was incubated with 100 ng of recombinant PTEN or GST-PTEN (labeled with *) for 1 min. PI(3,4)P_2 and PI(3)P were incubated with 1 μg of PTEN for 5 and 7 min, respectively. The GST-fusion protein shows essentially identical enzymatic activity with the nonfusion protein (data not shown).

(D) Normalized lipid phosphatase activity of human PTEN mutants. Initial rate of phosphoinositide phosphatase (PIPx ptase) activity toward PI(3,4,5)P_3, PI(3,4)P_2, and PI(3)P was divided by that of the pNPPase activity. The activity of wild-type PTEN toward each of the substrates is normalized to 100%. Other percentage activities represent ratios of wild-type versus mutants. n.d., not determined.

second anion-binding site adjacent to the catalytic phosphate-binding site.

Implications for PI(3,4,5)P_3 Binding

The 4.3 Å distance between the two carboxylate carbon atoms of tartrate is very similar to the 4.1 Å distance between the phosphorus atoms at the D3 and D4 positions of inositol (1,3,4,5)-tetrakisphosphate (Ins(1,3,4,5)P_4) (Baraldi et al., 1999). This suggests the model that PI(3,4,5)P_3 may bind with the D3 phosphate group at the catalytic site and the D4 phosphate group in the second anion-binding site. When the D3 and D4 phosphate groups of Ins(1,3,4,5)P_4 are superimposed on the carboxylate groups of tartrate, the D5 phosphate group occupies the remaining space in the pocket extension (Figures 3A and 3B). This results in a snug fit of the D3, D4, and D5 phosphate groups in the pocket without any steric clashes and without any adjustment in the Ins(1,3,4,5)P_4 structure obtained from the Protein Data Bank. In this superposition, the D5 phosphate group ends up next to the conserved Lys-128 and His-93 side chains. The D1 phosphate group ends up next to the conserved Lys-125, pointing away from the active site and available for attachment to the lipid (Figure 3B).

Mutagenesis of Pocket Residues

Because the pocket extension and the basic charge in the active site of PTEN distinguish it from known protein phosphatase structures, we mutated the residues responsible for these features and tested their effects on PTEN's PI(3,4,5)P_3 phosphatase activity.

On the "TI" loop, mutation of Thr-167 or Gln-171 resulted in reductions of 60% and 75%, respectively, in the activity of the enzyme toward PI(3,4,5)P_3 (Figure 3C). In the crystal structure, the Thr-167 side chain is solvent exposed and has no apparent structure-stabilizing role.

The Gln-171 side chain is partially solvent exposed and hydrogen bonds to one of the carboxylate groups of tartrate (Figure 2D). The reduction in the enzymatic activity resulting from their mutation thus suggests that the pocket extension where these residues occur plays an important role in PI(3,4,5)P_3 binding. In our PTEN–Ins(1,3,4,5)P_4 model, Thr-167 and Gln-171 are in the vicinity of the phosphate groups at the D4 and D5 positions (Figure 3B).

We next tested the effects of mutating the conserved basic residues in the PTEN active site. A Lys125Met mutation in the PTEN active site motif, H-C-K/R^{125}-A-G-K^{128}-G-R, resulted in a reduction of enzyme activity toward PI(3,4,5)P_3, as well as toward the poorer (Myers et al., 1998) substrates PI(3,4)P_2 and PI(3)P (Figure 3C). This result is consistent with our model, where Lys-125 would be in close proximity to the phosphate group at the D1 position. However, this mutation also reduced the phosphatase activity towards p-nitrophenyl phosphate (pNPP), a phosphatase substrate analog, and it is conceivable that Lys-125 may have additional roles. By contrast, mutation of Lys-128 to methionine reduced the PI(3,4,5)P_3 phosphatase activity by 85% while slightly elevating the pNPPase activity (Figure 3C). This mutation had a modest effect on PTEN activity with the other D3-phosphorylated substrates [PI(3,4)P_2 and PI(3)P] (Figure 3C). Data normalized against pNPPase activity clearly show that the reduction in the phosphatase activity is specific for the PI(3,4,5)P_3 substrate (Figure 3D). Among these substrates, only PI(3,4,5)P_3 has a phosphate group at the D5 position, and these data are consistent with an interaction between Lys-128 and the D5 phosphate group (Figure 3B). In support of this model, mutation of Lys-128 to an arginine did not reduce the enzymatic activity (Figure 3C).

Mutation of His-93 of the "WPD" loop had similar effects as the mutation of Lys-128, reducing the PI(3,4,5)P_3 phosphatase activity by 75% while having only a modest effect on the PI(3,4)P_2 phosphatase activity (Figure 3C). This result is also consistent with our model, where His-93 is in close proximity to the phosphate group at the D5 position (Figure 3B). This finding helps explain the high frequency of mutation of His-93 in cancer (Figure 1B).

Structure of the PTEN C2 Domain

The C-terminal 170 amino acids fold into a β sandwich structure consisting of two antiparallel β sheets with two short α helices intervening between the strands (Figures 1A and 1B). The PTEN β sandwich has a topology identical to the type II topology of the C2 fold, and its structure is similar to the C2 domains of PLCδ1, PKCδ, and phospholipase A2 (cPLA2) (Essen et al., 1996; Pappa et al., 1998; Perisic et al., 1998). It can be superimposed on the C2 domain of cPLA2 with an rms deviation of 1.9 Å for 85 Cα atoms, and with similar rms deviations on the PKCδ (1.7 Å/67 Cα) and PLCδ1 (1.9 Å/75 Cα) C2 domains (Figure 4A). These rms deviations are comparable to those reported between the more divergent members of the C2 family, such as the PKCδ and synaptotagmin C2 domains (1.7 Å/85 Cα) (Pappa et al., 1998).

The C2 domains of PLCδ1, PKCβ, cPLA2, and synaptotagmin I (SynI) can bind Ca^{2+} through three loops (CBR1, CBR2, and CBR3 loops) (reviewed by Rizo and Sudhof, 1998), and this has been implicated in mediating and regulating their membrane association (Essen et al., 1997; Perisic et al., 1998; Sutton and Sprang, 1998). The PTEN C2 domain differs from these C2 domains in that it lacks all but one (Asp-268) of the Ca^{2+} ligands and is thus unlikely to bind Ca^{2+}.

As it lacks the Ca^{2+} ligands, the PTEN C2 domain is unlikely to bind membranes in a Ca^{2+}-dependent manner. However, there are several analogies between the proposed membrane-interacting portions of the Ca^{2+}-dependent C2 domains and the corresponding regions of the PTEN C2 domain. PTEN has a CBR3 loop that has the same structure as in the Ca^{2+}-dependent C2 domains (Figures 4A and 6B). The structure of this loop extends perpendicularly away from the membrane-facing sheet of the Ca^{2+}-dependent C2 domains, and this structural feature has been suggested to play a central role in membrane binding (Essen et al., 1997; Perisic et al., 1998). The CBR3 loop of PTEN has a net +5 positive charge resulting from the solvent-exposed Lys-260, Lys-263, Lys-266, Lys-267, Lys-269, and the partially buried His-259–Asp-268 pair (Figures 1B and 4C). This positive charge could be similar to the positive charge resulting from Ca^{2+} binding to the CBR3 loops of the Ca^{2+}-dependent C2 domains, where the charge has been implicated in their affinity for the phospholipid phosphoryl groups (Essen et al., 1997). PTEN also contains two solvent-exposed hydrophobic residues, Met-264 and Leu-265, at the CBR3 tip (Figure 1B). This is a position where about half of the known C2 domains contain at least one hydrophobic residue (Perisic et al., 1998); based in part on fluorescence data with synaptotagmin (Chapman and Davis, 1998), the hydrophobic residue(s) has been proposed to insert into the lipid bilayer (Chapman and Davis, 1998; Bittova et al., 1999). Finally, the PTEN C2 domain has an additional basic patch on the adjacent cα2 helix, resulting from the solvent-exposed Lys-327, Lys-330, Lys-332, and Arg-335 (Figures 1B and 4C). This is a position similar to a helix of cPLA2 that has been implicated in contributing to membrane binding (Perisic et al., 1998).

These nine basic and two hydrophobic side chains emanating from the CBR3 and cα2 elements of the PTEN C2 domain are on the same face as and in close proximity to the phosphatase active site (Figure 4C), consistent with a possible role in membrane association.

C2 Domain Has Affinity for Phospholipid Membranes In Vitro

Because of these analogies, we tested whether the PTEN C2 domain has affinity for phospholipid membranes in vitro. We measured membrane binding using multilamellar phospholipid vesicles consisting of phosphatidyl choline (PC), according to published procedures (Davletov et al., 1998). Figure 4B shows that PTEN and the PTEN C2 domain fused to the GST protein bind the vesicles under conditions where several control proteins do not show detectable binding. In the positive control, the C2 domain of synaptotagmin bound the vesicles in a Ca^{2+}-dependent manner, as reported (Davletov and Sudhof, 1993). As expected, the in vitro membrane binding activity of PTEN does not require Ca^{2+}.

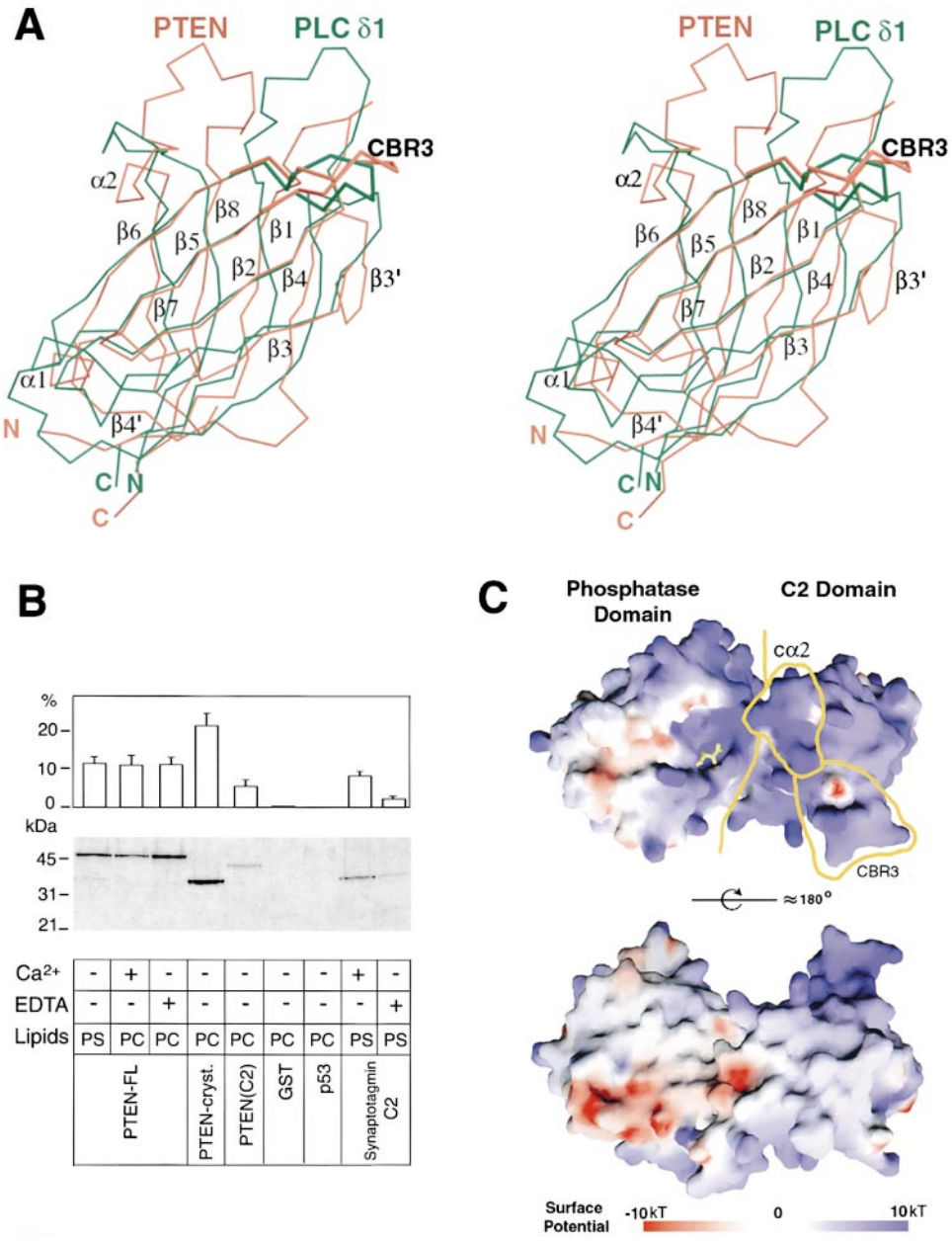

Figure 4. The C-Terminal Half of PTEN Has a C2 Domain of Type II Topology

(A) Stereo view of the Cα traces of the superimposed C2 domains of PTEN (red) and PLCδ1 (green).

(B) The PTEN C2 domain has affinity for phospholipid vesicles. Representative Coomassie-stained gel of proteins bound to pure phosphatidyl choline (PC) or phosphatidyl serine (PS) containing (at a PS:PE:PC ratio of 35:50:15) large multilamellar vesicles is shown. The lipid vesicles were prepared according to published procedures (Davletov et al., 1998). Bar graphs show the amount of bound protein relative to the total protein. PTEN-FL is full-length PTEN, PTEN-cryst. is the crystallized PTEN fragment, PTEN(C2) is a GST fusion protein of the PTEN C2 domain, and p53 is the DNA-binding domain of the p53 protein. PTEN(C2) has a tendency to aggregate, and this may contribute to its lower membrane binding activity in this assay. It is also conceivable that the phosphatase domain contributes to membrane binding. The isolated phosphatase domain could not be overexpressed in a soluble form. Where indicated, Ca^{2+} or EDTA was included at 2 mM.

(C) Surface electrostatic potential of PTEN. The top view is rotated ~90° about the horizontal axis of Figure 4A, so that the CBR3 loop is extending approximately out of the plane of the figure. Tartrate is in yellow.

Proposed Membrane-Binding Elements of the PTEN C2 Domain Are Important for Its Tumor Suppressor Function

To investigate the significance of PTEN's in vitro membrane affinity, we mutated the solvent-exposed residues in the CBR3 and cα2 elements of the C2 domain and tested the growth suppression activity of these PTEN mutants in vivo and their membrane affinity in vitro. In the M-CBR3 mutant, we replaced the sequence 263-K-M-L-K-K-D-K-269, which contains four of the five lysine

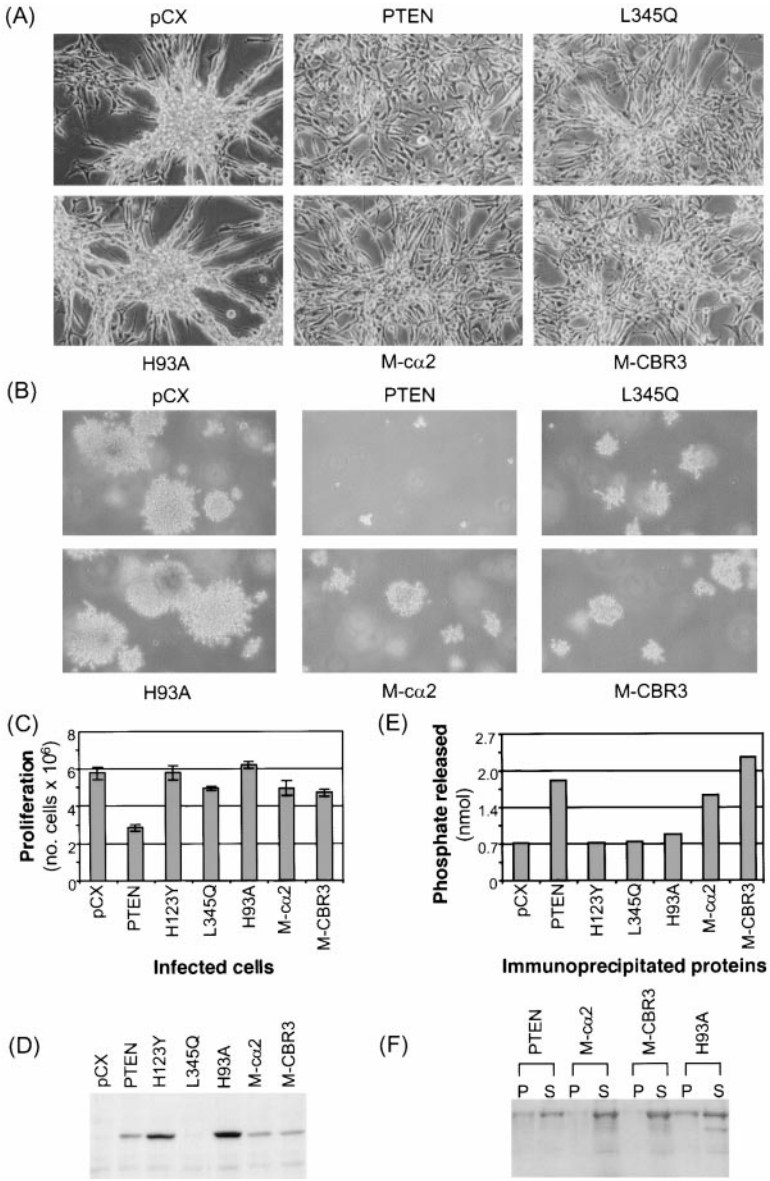

Figure 5. Inhibition of the Tumor Suppressor Activity of PTEN by Mutations in the Lipid-Binding C2 Regions

(A) Morphological changes and (B) anchorage-independent growth of retrovirus-infected U87-MG glioblastoma cells stably expressing PTEN and mutants. pCX is the retroviral vector without an insertion; PTEN is the wild-type PTEN; L345Q and H93A are tumor-derived mutations; M-cα2 and M-CBR3 contain the mutations described in the text. The photographs of the cells growing in plate and of the colonies developed in soft agar were taken at 20× and 10× magnification, respectively.

(C) Proliferation of the same cells. The number of retrovirus-infected cells surviving after the drug selection is shown. Infection efficiency of the virus was near 100%, and essentially no cells died during the drug selection.

(D) Protein expression levels for PTEN and mutants. Proteins (50 μg) from lysates of stably transfected U87-MG cells were resolved by SDS-polyacrylamide gel electrophoresis and analyzed by Western blotting with an anti-Myc antibody recognizing Myc-tagged PTEN and mutants.

(E) The $PI(3,4,5)P_3$-phosphatase activity of wild-type and mutant PTEN proteins immunoprecipitated from U87-MG cells using a short-chain, water-soluble $PI(3,4,5)P_3$. The amounts of immunoprecipitated proteins analyzed by Western blotting were comparable for wild-type PTEN, H93A, H123Y, M-cα2, and M-CBR3 mutants and were lower for the L345Q mutant (data not shown). These results were also reproduced with the recombinant GST-PTEN fusion proteins purified from *E. coli* (data not shown).

(F) M-cα2 and M-CBR3 mutants have reduced affinity for phospholipid vesicles. Representative Coomassie-stained gel of proteins bound to multilamellar vesicles containing phosphatidyl choline is shown. The lipid vesicles were prepared according to published procedures (Fukuda et al., 1996). The lanes labeled with P and S represent the pellet and supernatant fractions, respectively.

and both hydrophobic tip residues of the CBR3 loop, with the 263-A-A-G-A-A-D-A-269 sequence. The mutated residues are entirely solvent exposed and have no apparent structure-stabilizing roles. Asp-268 was not mutated, as it is partially buried and makes a salt bridge with His-259. In the M-cα2 mutant, we replaced the sequence 327-K-A-N-K-D-K-A-N-R-335 with 327-A-A-G-A-D-A-A-N-A-335, again none of the mutated residues having any apparent structure stabilizing roles. Asp-331 was not mutated, as it stabilizes a turn at the end of the cα2 helix through backbone hydrogen bonds and is also mutated in cancer.

The M-CBR3 and M-cα2 mutants were cloned in the pCX retroviral vector and stably expressed in U87-MG PTEN-deficient glioblastoma cells. For comparison, we also used the tumor-derived mutants His123Tyr of the phosphatase active site and Leu345Gln of the C2 domain hydrophobic core, both of which were previously studied with the same assay. As reported (Georgescu et al., 1999), the proliferation and anchorage-independent growth of U87-MG glioblastoma tumor cells were suppressed in the presence of wild-type PTEN, while the tumor-derived mutants His123Tyr and Leu345Gln allowed the growth of these cells (Figures 5A–5C). The cells expressing the His123Tyr mutant proliferated extensively in clusters lacking cell–cell contact inhibition and formed large colonies in the soft agar assay similar to control vector-transfected cells, while the Leu345Gln mutant in the C2 domain presented an intermediate tumor growth phenotype (Figures 5A–5C). The M-CBR3 and M-cα2 mutations reduced the growth suppression activity of PTEN to an extent comparable to that of the tumor-derived Leu345Gln mutant. The cells expressing the M-CBR3 and M-cα2 mutants proliferated better than wild-type PTEN-expressing cells and also lacked contact inhibition although not to the same extent as control cells (Figures 5A and 5C). When seeded in soft agar, these cells demonstrated anchorage-independent growth,

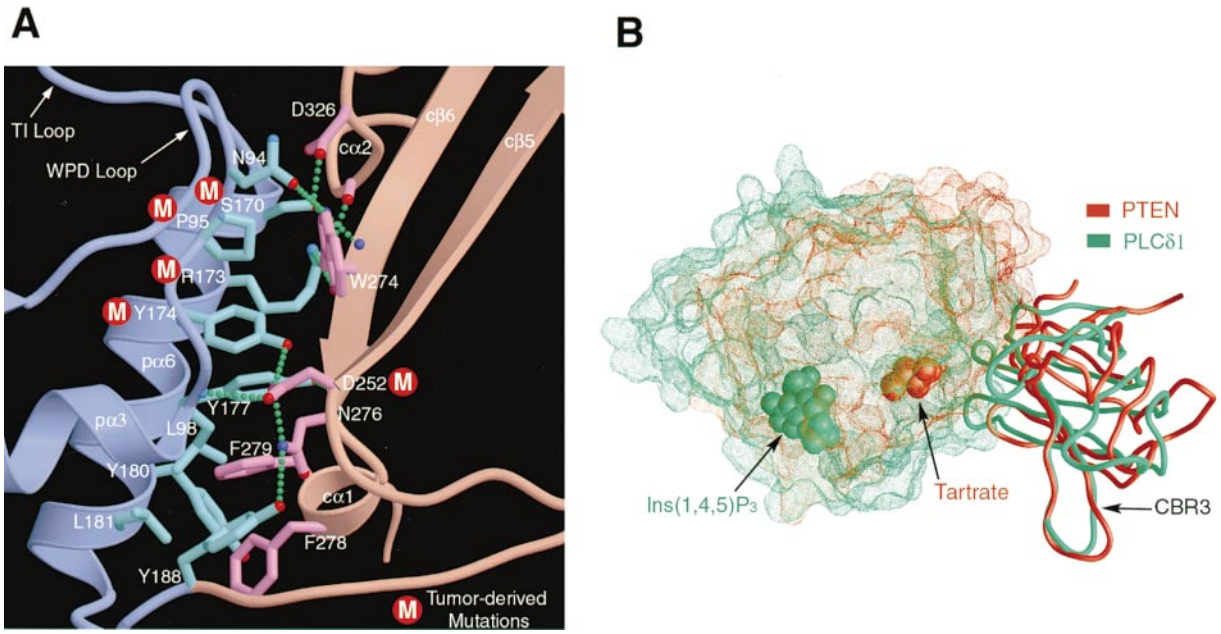

Figure 6. The PTEN Phosphatase and C2 Domains Pack across an Extensive Interface that Is Targeted by Tumorigenic Mutations

(A) The interface consists of the "WPD" loop, "TI" loop, and pα6 helix from the phosphatase domain (blue), and cβ5, cβ6, cα1, and cα2 from the C2 domain (magenta). The hydrogen bond networks in the interface are shown as green dotted lines.

(B) Superposition of PTEN (red) and PLCδ1 (green). Their C2 domains are shown as backbone traces, and their respective catalytic domains as dot surfaces. The active sites in both cases are located on the same face with the CBR3 loops.

giving rise to colonies of intermediate size between those formed by wild-type PTEN and the vector control (Figure 5B).

Because structural mutations in the C2 domain, such as Leu345Gln, were shown to induce the rapid degradation of PTEN in cells (Georgescu et al., 1999), we checked the expression level of our mutants in total cell lysates from the U87-MG cells. The M-CBR3 and M-cα2 mutants were present at levels essentially identical to that of wild-type PTEN (Figure 5D), indicating that the reduction in their growth suppression was not due to decreased protein levels in the cells. This also confirmed our structure-based conclusion that the residues we mutated do not have any structure-stabilizing roles. We also tested the ability of these PTEN mutants immunoprecipitated from cells to dephosphorylate a soluble, short-chain PI(3,4,5)P_3 analog, using published procedures (Georgescu et al., 1999). Figure 5E shows that the M-CBR3 and M-cα2 mutants have phosphatase activity levels similar to that of wild-type PTEN.

Finally, we tested the in vitro membrane binding affinity of the *E. coli* produced M-CBR3 and M-cα2 PTEN mutants using a published procedure (Fukuda et al., 1996) that is a variation of the procedure we used for the baculovirus-expressed PTEN. Figure 5F shows that these mutants have reduced affinity for membranes in vitro compared to *E. coli* produced wild-type PTEN.

Taken together, these results strongly suggest that PTEN binds to phospholipid membranes via its carboxy-terminal C2 domain and that its lipid binding activity is important for its tumor suppressor function. However, additional functions for the PTEN C2 domain, such as the protein binding demonstrated for one of the synaptotagmin C2 domains, cannot be ruled out.

We also tested the growth suppression activity of the tumor-derived His93Ala mutation, whose in vitro biochemical characterization indicated that His-93 may have a role in binding the D5 phosphate of PI(3,4,5)P_3. Cells expressing the His93Ala mutant proliferated extensively in clusters lacking cell–cell contact inhibition and formed large colonies in soft agar similar to control vector-transfected cells (Figures 5A–5C). Since this mutation reduced PTEN's in vitro PIP(3,4,5)P_3 phosphatase activity by 75% while preserving the phosphatase activity toward D3 phosphorylated phosphoinositides lacking the phosphate in the D5 position (Figure 3C), this result suggests that the dephosphorylation of PIP(3,4,5)P_3 is more important than the dephosphorylation of PIP(3,4)P_2 or PIP(3)P for the tumor suppressor function of PTEN.

Phosphatase–C2 Interface

The domain–domain interface buries a surface area of 1400 Å^2 and involves several structural elements from each domain, including parts of the "WPD" and "TI" loops of the phosphatase active site. The interface has seven hydrophobic and aromatic residues forming a buried core, and nine residues that participate in networks of hydrogen bonds, several of which are made with backbone groups (Figure 6A). The interface elements of the phosphatase domain are second only to the P loop in conservation across species (Figure 1B), and those of the C2 domain are the best conserved C2 regions (Figure 1B). The majority of the residues that make interdomain hydrogen bonds have been found mutated in cancer, and two of them, Ser-170 and Arg-173, are among the eight most frequently mutated residues of PTEN (Figures 1B and 6A). These indicate that the integrity of the interface is important for the function

Table 1. Statistics from the Crystallographic Analysis

Data Set	Native	Hg λ1	Hg λ2	Hg λ3
Wavelength (Å)	1.0000	1.0091	1.0081	0.9920
Resolution (Å)	2.1	2.7	2.7	2.7
Observations	188,143	108,117	108,062	108,067
Unique reflections	20,302	10,204	10,205	10,177
Data coverage (%)	95.8	98.3	98.4	98.1
R_{sym} (%)	3.7	4.8	5.4	6.0
MAD Analysis (10.0–3.0Å)				
Phasing power	0.70	—	0.48	0.84
R_{cullis}[a]	0.93	—	0.97	0.87
Anomalous R_{cullis}	—	0.76	0.77	0.80
Mean FOM		0.56		
Refinement Statistics				
Resolution (Å)	15.0–2.1			
Reflections[b]	20,302			
Protein atoms	2,578			
Water atoms	373			
R factor (%)[c]	21.9			
R_{free} (%)[d]	25.7			
Rmsd				
Bonds (Å)	0.010			
Angles (°)	1.68			
B factor (Å^2)	3.30			

[a]R_{cullis} is the mean residual lack of closure error divided by the dispersive or anomalous difference.
[b]Reflections, $|F| > 0\ \sigma$.
[c]R factor $= \Sigma\ |\ |F(obs)| - |F(calc)|\ |/\Sigma|F(obs)|$.
[d]R_{free} = R factor calculated using 5.0% of the reflection data chosen randomly and omitted from the start of refinement.

of PTEN. Consistent with these observations, the Asp-252Tyr tumor-derived mutation, which occurs on the C2 domain and would disrupt an interdomain hydrogen bond network (Figure 6A), causes an 85% reduction in the PI(3,4,5)P_3 phosphatase activity (data not shown).

The structural elements the PTEN C2 domain uses to interact with the phosphatase domain are very similar to the elements the PLCδ1 C2 domain uses to pack with its phospholipase domain (Figure 6B) (Essen et al., 1996). Furthermore, PTEN and PLCδ1 have a similar arrangement of their C2 domains relative to their active sites. In fact, when the two C2 domains are superimposed, the PTEN and PLCδ1 catalytic sites end up on the same side and within 10 Å of each other (Figure 6B). This suggests that the C2 domains in the two proteins may function similarly.

Homology to Tensin and Auxilin

The homology the PTEN phosphatase domain has with tensin and auxilin (Li et al., 1997; Steck et al., 1997), both of which lack key phosphatase active site residues, maps primarily to the hydrophobic core and to residues on the surface of the pα6 helix (Ser-170, Arg-173, Tyr-174, Tyr-177, and Leu-181). Since these pα6 helix residues pack with the C2 domain, their conservation raises the possibility that tensin and auxilin may also contain a C2 domain. In support of this hypothesis, we find that the sequence following the phosphatase fold of auxilin is most consistent with the structure of the PTEN C2 domain, among the nearly 2000 structures analyzed with the program THREADER2 (Miller et al., 1996). In this alignment, most of the PTEN C2 residues that interact with the phosphatase domain are similar in auxilin and tensin (Figure 1B).

Implications for PTEN Function

The structure reveals that PTEN has the dual specificity protein phosphatase fold but also has several active site characteristics that are divergent from those of DSPs and PTPs. These include the insertion in the "TI" loop, the P loop residues Gly-129, Lys-125, Lys-128, and the "WPD" loop residue His-93. These PTEN-specific features are evolutionarily conserved, are targeted by mutations in cancer, and their mutation reduces the PI(3,4,5)P_3 phosphatase activity of PTEN. Collectively, these observations indicate that the larger size and basic charge of the active site are important for PI(3,4,5)P_3 binding.

The structure also reveals that PTEN has a C2 domain, and in conjunction with our biochemical and growth suppression data with PTEN mutants, it suggests that this C2 domain may be involved in the association of PTEN with the membrane. It has been proposed that a three–amino acid sequence at the C terminus of PTEN may bind to PDZ domains and help recruit PTEN to the membrane (Teng et al., 1997), although the deletion of this sequence does not significantly affect the growth suppression activity of PTEN (Furnari et al., 1997; Georgescu et al., 1999). The presence of multiple membrane interaction modules would be reminiscent of many other C2-containing proteins, including PLCδ1 (Singer et al., 1997). In PLCδ1, the pleckstrin homology domain has been shown to contribute to the initial membrane recruitment, and the C2 domain has been suggested to fix the

position of the tightly linked catalytic domain on the membrane (Essen et al., 1996). The PTEN phosphatase and C2 domains are similarly tightly linked, and this suggests that the PTEN C2 domain not only may help recruit PTEN to the membrane, but it may also serve to position and orient the catalytic domain optimally with respect to the membrane-bound substrate. Our findings strongly support the model that the substrate important for the tumor suppressor function of PTEN is the membrane-bound PI(3,4,5)P_3.

Experimental Procedures

Protein Overexpression and Purification

Human PTEN containing residues 7–353 and an internal deletion of residues 286–309 was overexpressed using a baculovirus vector in Hi5 (Invitrogen) insect cells. It was purified by anion exchange, cation exchange, and gel filtration chromatography and was concentrated to ~20 mg/ml in 25 mM Tris-Cl, 0.4 M NaCl, 10 mM dithiothreitol (DTT) (pH 8.0). The full-length PTEN protein was prepared similarly.

The recombinant PTEN C2 domain (residues 183–353) and mutant PTEN proteins were overexpressed in *E. coli* as glutathione S-transferase (GST) fusion proteins, and they were purified by glutathione-Sepharose (Pharmacia) affinity chromatography. K125M, K128M, and K128R mutants were further purified as described (Maehama and Dixon, 1998). The cytosolic domain of synaptotagmin-I (Chapman and Jahn, 1994) was overexpressed as a GST fusion protein, cleaved with thrombin, and purified by anion exchange chromatography.

Crystallization and Data Collection

Crystals were grown at room temperature by the hanging-drop vapor diffusion method from 1.3 M Na/K L(+)-tartrate, 5%–10% (v/v) glycerol, 100 mM Tris-Cl, 10 mM DTT (pH 8.0). They form in space group I4 with a = b = 113.2 Å, c = 56.9 Å and contain one molecule in the asymmetric unit. The native data set was collected using crystals flash frozen in crystallization buffer supplemented with 25% glycerol at −170°C. The structure was determined using the multiwavelength anomalous diffraction (MAD) method with mercury-derivatized crystals (Table 1). For the MAD data sets, crystals were pretreated with 0.25% (v/v) glutaraldehyde for 30 min to reduce their tendency to crack and were soaked in 2 mM thimerosal for 1 hr before being frozen.

Structure Determination and Refinement

Phasing was done by treating MAD as a special case of MIR. The initial phases, calculated at 3.0 Å resolution with the program MLPHARE (Table 1), were improved by density modification with the program DM (Collaborative Computational Project, 1994). An initial model, built with the program O (Jones et al., 1991), was improved by several cycles of manual rebuilding and refinement with the program CNS (Brünger et al., 1998). A strong (>3 σ), continuous Fo-Fc electron density in the active site could be modeled in its entirety as an L(+)-tartrate molecule. In the refined model, the tartrate molecule has an overall temperature factor of 29.8 Å^2, compared to 43.0 Å^2 for the overall PTEN phosphatase domain. Amino acids 7–13, 282–285, and 352–353 are not visible in the electron density maps and are presumed to be disordered.

Protein Binding to Large Multilamellar Vesicles

Five-microgram aliquots of the proteins were mixed with 100 μg of large multilamellar vesicles, prepared according to either one of the published procedures (Fukuda et al., 1996; Davletov et al., 1998), in a buffer containing 50 mM Tris-Cl, 150 mM NaCl, 10 mM DTT, 0.001% Triton X-100 (pH 8.0). After 15 min of incubation at room temperature, the mixtures were centrifuged at 11,600 × g for 10 min, and the pellets containing lipid and bound proteins were separated on SDS–PAGE gels. The proteins in the supernatant fractions were precipitated with 10% trichloroacetic acid and washed twice with acetone before loading.

Phosphatase Assays

Lipid phosphatase assays were performed by the incubation of 100 μM PI (3,4,5)P_3, PI(3,4)P_2, PI(3)P (BIOMOL) with purified recombinant PTEN in a 10 μl reaction mixture consisting of 100 mM Tris-HCl (pH 8), 10 mM DTT, 1 mM phosphatidylserine at 37°C. The reactions were terminated by addition of 15 μl of ice-cold 100 mM N-ethylmaleimide, and phospholipids were precipitated by centrifugation (10,000 × g, 15 min). Twenty microliters of the cleared supernatant was mixed with 80 μl of GREEN reagent (BIOMOL), and the concentration of released phosphate was determined by measuring of OD at 620 nm after 20 min of incubation at room temperature. Phosphatase activity of PTEN toward p-nitrophenylphosphate (pNPP) was determined as described (Maehama and Dixon, 1998). The phosphatase assay using water-soluble diC_8-PI(3,4,5)P_3 (Echelon) and proteins immunoprecipitated from U87-MG cells with 1 μg anti-Myc 9E10 antibody (Calbiochem) was done as described (Georgescu et al., 1999).

Cells, Transfection, Proliferation Assay, and Apoptosis Assay

Wild-type PTEN and the mutants were cloned in-frame with an N-terminal Myc tag in the pCX retroviral vector (Georgescu et al., 1999). U-87 MG glioblastoma cell line (ATCC) and Bosc23 retrovirus-packaging cells were grown in Dulbecco's modified Eagle's medium with 10% fetal calf serum. The transfection of the Bosc23 cells followed by the infection of U-87 MG glioblastoma cells with the retrovirus-containing supernatants and the drug selection of stable PTEN-expressing cells were done as described (Georgescu et al., 1999). For the proliferation assay, the cells growing in the 6 cm dishes after complete selection were trypsinized and counted using a hemocytometer. The soft agar colony assay was performed as described (Georgescu et al., 1999), and the size of colonies was recorded 2 weeks after seeding. The protein expression levels were assayed in total cell lysates by Western blotting with anti-Myc antibody (Invitrogen).

For the apoptosis assay, LNCaP human prostate carcinoma cell line was transfected with wild-type or the crystallized fragment of PTEN in pcDNA3.1, in the presence of a β-gal expression construct. Forty-eight hours after transfection, the cells were fixed as described (Wang et al., 1999), and blue cells were scored under a microscope.

Acknowledgments

We thank S. Geromanos and H. Erdjument-Bromage of the Sloan-Kettering Microchemistry Facility for N-terminal sequence and mass spectroscopic analyses; the staff of the Cornell High Energy Synchrotron Source (MacChess) for help with data collection; T. Weber for advice about the lipid binding assay; and C. Murray for administrative help. This work was supported by the Howard Hughes Medical Institute, the National Institutes of Health, the Dewitt Wallace Foundation, the Samuel and May Rudin Foundation, and the Walther Cancer Institute. M. M. G. was supported by fellowships from the Medical Research Council of Canada and the National Cancer Institute (CA09673). P. P. is a scholar of the Leukemia Society of America.

Received August 25, 1999; revised September 23, 1999.

References

Altschul, S.F., Madden, T.L., Schaffer, A.A., Zhang, J., Zhang, Z., Miller, W., and Lipman, D.J. (1997). Gapped BLAST and PSI-BLAST: a new generation of protein database search programs. Nucleic Acids Res. *25*, 3389–3402.

Baraldi, E., Carugo, K.D., Hyvonen, M., Surdo, P.L., Riley, A.M., Potter, B.V., O'Brien, R., Ladbury, J.E., and Saraste, M. (1999). Structure of the PH domain from Bruton's tyrosine kinase in complex with inositol 1,3,4,5-tetrakisphosphate. Structure *7*, 449–460.

Barford, D., Flint, A.J., and Tonks, N.K. (1994). Crystal structure of human protein tyrosine phosphatase 1B. Science *263*, 1397–1404.

Bittova, L., Sumandea, M., and Cho, W. (1999). A structure-function study of the C2 domain of cytosolic phospholipase A2. Identification of essential calcium ligands and hydrophobic membrane binding residues. J. Biol. Chem. *274*, 9665–9672.

Brünger, A.T., Adams, P.D., Clore, G.M., DeLano, W.L., Gros, P.,

Grosse-Kunstleve, R.W., Jiang, J.S., Kuszewski, J., Nilges, M., Pannu, N.S., et al. (1998). Crystallography and NMR system: a new software suite for macromolecular structure determination. Acta Crystallogr. D Biol. Crystallogr. *54*, 905–921.

Chapman, E.R., and Davis, A.F. (1998). Direct interaction of a Ca^{2+}-binding loop of synaptotagmin with lipid bilayers. J. Biol. Chem. *273*, 13995–14001.

Chapman, E.R., and Jahn, R. (1994). Calcium-dependent interaction of the cytoplasmic region of synaptotagmin with membranes. Autonomous function of a single C2-homologous domain. J. Biol. Chem. *269*, 5735–5741.

Collaborative Computational Project, Number 4 (1994). The CCP4 suite: programs for protein crystallography. Acta Crystallogr. D *50*, 760–763.

Davletov, B.A., and Sudhof, T.C. (1993). A single C2 domain from synaptotagmin I is sufficient for high affinity Ca^{2+}/phospholipid binding. J. Biol. Chem. *268*, 26386–26390.

Davletov, B., Perisic, O., and Williams, R.L. (1998). Calcium-dependent membrane penetration is a hallmark of the C2 domain of cytosolic phospholipase A2 whereas the C2A domain of synaptotagmin binds membranes electrostatically. J. Biol. Chem. *273*, 19093–19096.

Di Cristofano, A., Pesce, B., Cordon-Cardo, C., and Pandolfi, P.P. (1998). Pten is essential for embryonic development and tumour suppression. Nat. Genet. *19*, 348–355.

Essen, L.O., Perisic, O., Cheung, R., Katan, M., and Williams, R.L. (1996). Crystal structure of a mammalian phosphoinositide-specific phospholipase C delta. Nature *380*, 595–602.

Essen, L.O., Perisic, O., Lynch, D.E., Katan, M., and Williams, R.L. (1997). A ternary metal binding site in the C2 domain of phosphoinositide-specific phospholipase C-δ1. Biochemistry *36*, 2753–2762.

Fukuda, M., Kojima, T., and Mikoshiba, K. (1996). Phospholipid composition dependence of Ca^{2+}-dependent phospholipid binding to the C2A domain of synaptotagmin IV. J. Biol. Chem. *271*, 8430–8434.

Furnari, F.B., Lin, H., Huang, H.S., and Cavenee, W.K. (1997). Growth suppression of glioma cells by PTEN requires a functional phosphatase catalytic domain. Proc. Natl. Acad. Sci. USA *94*, 12479–12484.

Furnari, F.B., Huang, H.J., and Cavenee, W.K. (1998). The phosphoinositol phosphatase activity of PTEN mediates a serum-sensitive G1 growth arrest in glioma cells. Cancer Res. *58*, 5002–5008.

Georgescu, M.-M., Kirsch, K.H., Akagi, T., Shishido, T., and Hanafusa, H. (1999). The tumor suppressor activity of PTEN is regulated by its carboxy-terminal region. Proc. Natl. Acad. Sci. USA *96*, 10182–10187.

Jia, Z., Barford, D., Flint, A.J., and Tonks, N.K. (1995). Structural basis for phosphotyrosine peptide recognition by protein tyrosine phosphatase 1B. Science *268*, 1754–1758.

Jones, T.A., Zou, J.Y., Cowan, S.W., and Kjeldgaard, M. (1991). Improved methods for binding protein models in electron density maps and the location of errors in these models. Acta Crystallogr. A *47*, 110–119.

Li, D.M., and Sun, H. (1998). PTEN/MMAC1/TEP1 suppresses the tumorigenicity and induces G1 cell cycle arrest in human glioblastoma cells. Proc. Natl. Acad. Sci. USA *95*, 15406–15411.

Li, J., Yen, C., Liaw, D., Podsypanina, K., Bose, S., Wang, S.I., Puc, J., Miliaresis, C., Rodgers, L., McCombie, R., et al. (1997). PTEN, a putative protein tyrosine phosphatase gene mutated in human brain, breast, and prostate cancer. Science *275*, 1943–1947.

Maehama, T., and Dixon, J.E. (1998). The tumor suppressor, PTEN/MMAC1, dephosphorylates the lipid second messenger, phosphatidylinositol 3,4,5-trisphosphate. J. Biol. Chem. *273*, 13375–13378.

Maehama, T., and Dixon, J.E. (1999). PTEN: a tumour suppressor that functions as a phospholipid phosphatase. Trends Cell Biol. *9*, 125–128.

Miller, R.T., Jones, D.T., and Thornton, J.M. (1996). Protein fold recognition by sequence threading: tools and assessment techniques. FASEB J. *10*, 171–178.

Myers, M.P., Stolarov, J.P., Eng, C., Li, J., Wang, S.I., Wigler, M.H., Parsons, R., and Tonks, N.K. (1997). P-TEN, the tumor suppressor from human chromosome 10q23, is a dual-specificity phosphatase. Proc. Natl. Acad. Sci. USA *94*, 9052–9057.

Myers, M.P., Pass, I., Batty, I.H., Van der Kaay, J., Stolarov, J.P., Hemmings, B.A., Wigler, M.H., Downes, C.P., and Tonks, N.K. (1998). The lipid phosphatase activity of PTEN is critical for its tumor supressor function. Proc. Natl. Acad. Sci. USA *95*, 13513–13518.

Ogg, S., and Ruvkun, G. (1998). The *C. elegans* PTEN homolog, DAF-18, acts in the insulin receptor-like metabolic signaling pathway. Mol. Cell *2*, 887–893.

Pappa, H., Murray-Rust, J., Dekker, L.V., Parker, P.J., and McDonald, N.Q. (1998). Crystal structure of the C2 domain from protein kinase C-δ. Structure *6*, 885–894.

Perisic, O., Fong, S., Lynch, D.E., Bycroft, M., and Williams, R.L. (1998). Crystal structure of a calcium-phospholipid binding domain from cytosolic phospholipase A2. J. Biol. Chem. *273*, 1596–1604.

Podsypanina, K., Ellenson, L.H., Nemes, A., Gu, J., Tamura, M., Yamada, K.M., Cordon-Cardo, C., Catoretti, G., Fisher, P.E., and Parsons, R. (1999). Mutation of Pten/Mmac1 in mice causes neoplasia in multiple organ systems. Proc. Natl. Acad. Sci. USA *96*, 1563–1568.

Rizo, J., and Sudhof, T.C. (1998). C2-domains, structure and function of a universal Ca^{2+}-binding domain. J. Biol. Chem. *273*, 15879–15882.

Singer, W.D., Brown, H.A., and Sternweis, P.C. (1997). Regulation of eukaryotic phosphatidylinositol-specific phospholipase C and phospholipase D. Annu. Rev. Biochem. *66*, 475–509.

Stambolic, V., Suzuki, A., de la Pompa, J.L., Brothers, G.M., Mirtsos, C., Sasaki, T., Ruland, J., Penninger, J.M., Siderovski, D.P., and Mak, T.W. (1998). Negative regulation of PKB/Akt-dependent cell survival by the tumor suppressor PTEN. Cell *95*, 29–39.

Steck, P.A., Pershouse, M.A., Jasser, S.A., Yung, W.K., Lin, H., Ligon, A.H., Langford, L.A., Baumgard, M.L., Hattier, T., Davis, T., et al. (1997). Identification of a candidate tumour suppressor gene, MMAC1, at chromosome 10q23.3 that is mutated in multiple advanced cancers. Nat. Genet. *15*, 356–362.

Stuckey, J.A., Schubert, H.L., Fauman, E.B., Zhang, Z.Y., Dixon, J.E., and Saper, M.A. (1994). Crystal structure of Yersinia protein tyrosine phosphatase at 2.5 Å and the complex with tungstate. Nature *370*, 571–575.

Sun, H., Lesche, R., Li, D.M., Liliental, J., Zhang, H., Gao, J., Gavrilova, N., Mueller, B., Liu, X., and Wu, H. (1999). PTEN modulates cell cycle progression and cell survival by regulating phosphatidylinositol 3,4,5,-trisphosphate and Akt/protein kinase B signaling pathway. Proc. Natl. Acad. Sci. USA *96*, 6199–6204.

Sutton, R.B., and Sprang, S.R. (1998). Structure of the protein kinase Cβ phospholipid-binding C2 domain complexed with Ca^{2+}. Structure *6*, 1395–1405.

Suzuki, A., de la Pompa, J.L., Stambolic, V., Elia, A.J., Sasaki, T., del Barco Barrantes, I., Ho, A., Wakeham, A., Itie, A., Khoo, W., et al. (1998). High cancer susceptibility and embryonic lethality associated with mutation of the PTEN tumor suppressor gene in mice. Curr. Biol. *8*, 1169–1178.

Tamura, M., Gu, J., Matsumoto, K., Aota, S., Parsons, R., and Yamada, K.M. (1998). Inhibition of cell migration, spreading, and focal adhesions by tumor suppressor PTEN. Science *280*, 1614–1617.

Teng, D.H., Hu, R., Lin, H., Davis, T., Iliev, D., Frye, C., Swedlund, B., Hansen, K.L., Vinson, V.L., Gumpper, K.L., et al. (1997). MMAC1/PTEN mutations in primary tumor specimens and tumor cell lines. Cancer Res. *57*, 5221–5225.

Wang, J., Zheng, L., Lobito, A., Chan, F.K., Dale, J., Sneller, M., Yao, X., Puck, J.M., Straus, S.E., and Lenardo, M.J. (1999). Inherited human Caspase 10 mutations underlie defective lymphocyte and dendritic cell apoptosis in autoimmune lymphoproliferative syndrome type II. Cell *98*, 47–58.

Yuvaniyama, J., Denu, J.M., Dixon, J.E., and Saper, M.A. (1996). Crystal structure of the dual specificity protein phosphatase VHR. Science *272*, 1328–1331.

Protein Data Bank ID Code

The coordinates for the structure described in this work have been deposited with the ID code 1d5r.

GenBank Accession Number

The GenBank accession number of *Xenopus PTEN* is AF144732.